EasyChair Preprint

№ 14538

Numerical Investigation of Non-Premixed Hydrogen Flame Dynamics Using RANS Models

Hafidz Jakaria, Naef Qasem and Binash Imteyaz

August 26, 2024

Numerical investigation of non-premixed hydrogen flame dynamics using RANS models

Hafidz Azhar Jakaria, Naef A.A. Qasem, Binash A. Imteyaz

Abstract

Hydrogen has sparked major stakeholders as an alternative to fossil fuel in industrial gas turbines or aerospace applications, considering its clean energy to reduce greenhouse gas emissions. Furthermore, hydrogen is known to have higher gravimetric energy density than conventional fuel. However, understanding hydrogen flames is particularly challenging due to the intricate nature of the turbulence characteristics. Hence, non-premixed turbulent hydrogen flames are numerically investigated in this work using ANSYS Fluent with and without a user-defined function. This work aims to assess the predictability of various RANS turbulence models for an axisymmetric case, including standard, modified, realizable, and Pope correction models. Simulation of test cases has shown that the realizable model exhibits the best accuracy in the centerline region further downstream with high accuracy for the centerline mean temperature. The modified model demonstrates superior predictability near the injector exit plane in the radial direction. Overall, the findings suggest that RANS models are effective for initial data collection in the early stages of the design process, providing valuable insights into the behavior of hydrogen flames.

Keywords: Hydrogen flames; Numerical; RANS; Non-premixed turbulent flame; User-defined function

Nomenclature

CMC	Conditional moment closure
EDC	Eddy dissipation concept
EPDF	Eulerian probability density function
LES	Large eddy simulation
PDF	Probability density function
PEUL	Probabilistic Eulerian-Lagrangian
RSM	Reynolds stress model
RANS	Reynolds-averaging Navier-Stokes
TKE	Turbulent kinetic energy
UDF	User-defined function

1. Introduction

In recent years, hydrogen fuel has been tremendously popular among the stakeholders in the transition toward renewable green energy, considering its ability and potential to decrease greenhouse gases. Unlike conventional fuels, hydrogen combustion theoretically produces only water vapor as a byproduct, a promising approach for eliminating carbon dioxide emissions. However, the feasibility of fully applied hydrogen combustion in commercial industries is a bit stretched, given its numerous obstacles. For instance, turbulent hydrogen flames are famously complicated, where the intricate dynamics between chemistry and turbulent combustion are major factors (Fiorina 2019). Furthermore, hydrogen storage, production, and maintenance costs are several conspicuous challenges to investigating its combustion characteristics practically (Habib et al. 2024). Therefore, numerical models offer a great practical approach to simulate a reacting turbulent flow in engineering applications.

Accurate simulation and prediction of combustion characteristics in a turbulent reacting flow requires the consideration of multiple crucial factors, including turbulence model, combustion-chemistry model, chemical kinetic, boundary conditions, and radiation model. Tabet-Helal et al. (2006) studied the prediction of turbulence hydrogen flames using a steady strained laminar flamelet model. Two turbulence models, the k-ε model and the Reynolds stress model (RSM), were compared, with the inclusion of pope correction in both turbulence methods. Moreover, the PDF

combustion model was also adopted with H2O as the radiating species. His study concluded that both k-ε and RSM can predict hydrogen flames at atmospheric pressure. The RSM model shows better agreement with the experimental data when closer to the injector exit plane, while downstream, k-ε shows high accuracy. In his further work (Tabet et al. 2011), simulations were done in various elevated pressures (1-10atm), using the k-ε turbulence model with pope correction, steady flamelet, and PDF model. Oumrani et al. (2015) validated the modified k-ε and RSM model with $C_{\varepsilon 2}$=1.82 of the turbulent hydrogen flames without applying pope correction. His study showed that these two modified models give comparable results of earlier investigations. Larbi et al. (2018) applied the Eulerian probability density function (EPDF) to investigate its effect on turbulent lifted hydrogen diffusion flame in a Vitiated Coflow. GRI mech 2.1. the mechanism was chosen to solve the chemical reaction mechanism. A modified standard k-ε ($C_{\varepsilon 1}$=1.55) and RSM models were chosen to solve the turbulent transport. In this investigation, indeed, RSM predicts better result than the k-ε model; however, in the case of a round jet, it is easier to control k-ε constant parameters to yield a better result.

In the present work, a turbulence round jet hydrogen flame is modeled using different RANS turbulence models, namely the standardized k-ε model developed by Launder & Spalding (1979), the modified k-ε model ($C_{\varepsilon 1}$=1.6), the realizable k-ε model developed by Shih et al. (1995), and k-ε model with pope correction (Pope 1978). The aim of this study is simply to analyze whether the limited k-ε model presents good predictions against experimental data and reproduced k-ε with a Pope correction approach at the axial profile and radial. A steady laminar flamelet developed by Pitsch & Peters (1998) is employed given the flame is fully turbulent. Moreover, the PDF combustion model is adopted, and H_2O is chosen as the radiating species.

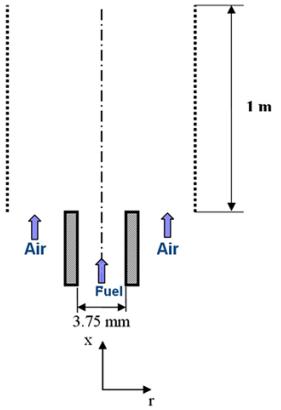

Fig. 1. Flame setup, inner fuel injector diameter = 3.75mm, outer fuel injector diameter = 4.8mm, and far-field axial distance = 1m.

2. Numerical Setup

2.1. Computational domain and boundary conditions

The non-premixed vertical turbulent hydrogen flame was modeled and verified against the experimental data of Barlow & Carter (1994) for temperature and species concentrations. In their test rig, an undiluted hydrogen fuel was injected via a straight tube with an inner diameter of 3.75 mm and an outer diameter of 4.8 mm, which was located at the center of a vertical wind tunnel exit. The fuel injector was surrounded by coflowing air stemming from a wind tunnel. The hydrogen flame is said to have a length (L) of 675mm. In the present study, the computational domain starts at the exit plane of the fuel injector, extending it to 1m downstream in the axial direction and 0.3m in the radial direction, as shown in Fig. 1. The flow domain and mixing fields are assumed to be 2D axisymmetric solved by k-ε turbulence model. The air inlet is set to 1m/s while the fuel inlet is set to 296m/s. The operating condition for this simulation is set to atmospheric pressure and room temperature. Measurement locations are normalized against the flame length, as shown in Table 1. In this study, ANSYS Fluent was used to solve the numerical simulation of two-

dimensional axisymmetric reacting flow using the finite volume method. The Coupled numerical scheme was used to solve the velocity and pressure coupling. The least squares cell-based and second-order schemes were selected to discretize the spatial gradient and pressure, respectively. The second-order upwind method has opted to discretize all the other terms.

Table 1. Absolute and normalized measurement locations

Axial position (X/L_{flame})	mm
1/8	84
1/2	338
1/1	675

2.2. Governing equations

To model hydrogen turbulent combustion, the governing equations used are conservation of mass, momentum, energy, and species, besides the chemical reaction and kinetics and turbulent model. Reynolds averaging governs the instantaneous Navier-Stokes equation into mean flow quantities. Conservation of mass can be expressed as follows (Chen & Ghoniem 2012)]:

$$\frac{\partial \bar{\rho}}{\partial t} + \frac{\partial}{\partial x_i}(\bar{\rho}\,\tilde{u}_i) = 0 \tag{1}$$

where $\bar{\rho}$ represents the averaged density and $\tilde{u}_i$ is the velocity vector. The conservation of momentum is formulated as follows:

$$\frac{\partial(\bar{\rho}\,\tilde{u}_i)}{\partial t} + \frac{\partial(\bar{\rho}\,\tilde{u}_i\tilde{u}_j)}{\partial x_j} = -\frac{\partial \bar{p}}{\partial x_i} + \frac{\partial}{\partial x_j}\left[\mu\left(\frac{\partial \tilde{u}_i}{\partial x_j} + \frac{\partial \tilde{u}_j}{\partial x_i} - \frac{2}{3}\delta_{ij}\frac{\partial \tilde{u}_k}{\partial x_k}\right)\right] + \frac{\partial}{\partial x_j}\left(-\overline{\rho u_i' u_j'}\right) \tag{2}$$

where Favre-averaged velocity components are represented by $\tilde{u}_i$, $\tilde{u}_j$, and $\tilde{u}_k$; the fluctuations are denoted by u_i' and u_j'; $\bar{\rho}$ and $\bar{p}$ are defined as the time-averaged density and statistic pressure, respectively; μ is the molecular viscosity. The expression of $\left(-\overline{\rho u_i' u_j'}\right)$ is described as the Reynold stresses, which can be solved using the following equation:

$$\frac{\partial(\bar{\rho}k)}{\partial t} + \frac{\partial(\bar{\rho}k\tilde{u}_i)}{\partial x_i} = \frac{\partial}{\partial x_j}\left[\left(\mu + \frac{\mu_t}{\sigma_k}\right)\frac{\partial k}{\partial x_j}\right] + G_k + G_b - \rho\varepsilon - Y_M + S_k \tag{3}$$

$$\frac{\partial(\bar{\rho}\varepsilon)}{\partial t} + \frac{\partial(\bar{\rho}\varepsilon\tilde{u}_i)}{\partial x_i} = \frac{\partial}{\partial x_j}\left[\left(\mu + \frac{\mu_t}{\sigma_\varepsilon}\right)\frac{\partial \varepsilon}{\partial x_j}\right] + C_{1\varepsilon}\frac{\varepsilon}{k}(G_k + C_{\varepsilon b}G_b) - C_{2\varepsilon}\bar{\rho}\frac{\varepsilon^2}{k} + S_\varepsilon \tag{4}$$

In this formula, the term k is defined as turbulence kinetic energy, the term ε is dissipation rate, the symbol μ is defined as the laminar dynamic viscosity, G_k and G_b refer to the production of turbulence kinetic energy because of averaged velocity gradients and buoyancy, respectively, Y_M is the fluctuating dilatation contribution. S_k and S_ε represent the user-defined source terms. Eqs. (3) and (4) are considered the standard *k-ε* turbulent models. Other *k-ε* turbulent models, such as the realizable model, have similar forms but with slight differences, including turbulent Prandtl numbers and terms in dissipation rate (ANSYS 2021). In this study, the detailed constants parameter ($C_{1\varepsilon}$ and $C_{2\varepsilon}$) for RANS turbulence models for simulation are depicted in Table 2.

In the present work, a user-defined function (UDF) is used to add a source term for the dissipation rate is added by using the Pope correction. This method improves the prediction of the spreading rate of a round jet in a standard *k-ε* model (Pope 1978). Pope's correction may be formulated as:

$$S_{PC} = C_{\varepsilon 3}\rho\frac{\varepsilon^2}{k}\chi_p \tag{5}$$

where $C_{\varepsilon 3} = 0.79$. For an axisymmetric flow, χ_p is defined as:

$$\chi_p = \frac{1}{4}\left(\frac{k}{\varepsilon}\right)^3\left(\frac{\partial u}{\partial y} - \frac{\partial v}{\partial x}\right)^2\frac{v}{r_c} \tag{6}$$

where r_c is described as the distance from the centerline of the flow.

The mathematical model for energy transport with radiation source term can be expressed as (Peters 2001):

$$\frac{\partial}{\partial t}\left(\bar{\rho}\tilde{H}\right) + \frac{\partial}{\partial x_i}\left(\bar{\rho}\tilde{u}_i\tilde{H}\right) = \frac{\partial}{\partial x_i}\left(\frac{\mu_t}{Pr_t}\frac{\partial \tilde{H}}{\partial x_i}\right) + S_h \tag{7}$$

where $\widetilde{H}$ is the mean enthalpy, Pr_t is the Prandtl number, and S_h is the radiation source term. Prandtl number is set to 0.85 (ANSYS 2021).

In this work, the discrete ordinates (DO) radiation model solves the radiative transfer equation (RTE). The DO model is applicable to a wide variety of optical thicknesses of gases. The radiation equation may be formulated as follows:

$$S_h = \alpha \left(\int_{4\pi} I(r, \Omega) \mathrm{d}\Omega - \sigma T^4 \right) \tag{8}$$

where α is the absorption coefficient, I is the spectral radiation intensity with the function position and direction, σ is the Steffan-Boltzmann constant ($5.6704 \times 10^{-8} W/m^2 \cdot K^4$), and T is the temperature. In this work, the considered radiating species is H_2O.

Table 2. Turbulence models presented in this study, including its label name

Turbulence model	Label name	$C_{\varepsilon 1}$	$C_{\varepsilon 2}$
Standard k-ε	Std-KE	1.44	1.92
Modified k-ε	Mod-KE	1.6	1.92
Realizable k-ε	Realizable-KE	-	1.9
Pope correction k-ε	PC-KE	1.44	1.92

2.3. Chemistry and combustion

A term mixture fraction (f) can represent the equation for different chemical species under the assumption of equal diffusivities. Indeed, equal diffusivities pose challenges for laminar flows, but it is deemed acceptable for turbulent flows. The transport equation for the Favre-averaged mixture fraction ($\bar{f}$) and its variance ($\overline{f'^2}$) can be expressed as (ANSYS 2021):

$$\frac{\partial}{\partial t}\left(\rho \bar{f}\right) + \nabla \cdot \left(\rho \vec{v} \bar{f}\right) = \nabla \cdot \left(\left(\frac{k_l}{c_p} + \frac{\mu_t}{\sigma_t} \right) \nabla \bar{f} \right) + S_m \tag{9}$$

$$\frac{\partial}{\partial t}\left(\rho \overline{f'^2}\right) + \nabla \cdot \left(\rho \vec{v} \overline{f'^2}\right) = \nabla \cdot \left(\left(\frac{k}{c_p} + \frac{\mu_t}{\sigma_t} \right) \nabla \overline{f'^2} \right) + C_g \mu_t \cdot \left(\nabla \bar{f}\right)^2 - C_d \rho \frac{\varepsilon}{k} \overline{f'^2} \tag{10}$$

where k_l is defined as the laminar thermal conductivity, the term C_p is the specific heat of the mixture, and S_m is a source term for the mass transfer of liquid fuel droplets to the gas phase. $\sigma_t = 0.85$, $C_g = 2.86$, and $C_d = 2.0$. The density-weighted thermochemical scalars (species mass fractions and temperature) are calculated using the following equation:

$$\bar{\phi} = \int \int \phi\,(f, \chi_{st}) p(f, \chi_{st}) df d\chi_{st} \tag{11}$$

where the term ϕ symbolizes the species mass fractions and temperature. The probability density function $p(f)$ is solved using the *beta-PDF* assumption using the following expression:

$$p(f) = \frac{f^{\alpha-1}(1-f)^{\beta-1}}{\int f^{\alpha-1}(1-f)^{\beta-1} df} \tag{12}$$

The mean scalar dissipation can be formulated as:

$$\overline{\chi_{st}} = \frac{C_\chi \varepsilon \overline{f'^2}}{k} \tag{13}$$

Constant $C_\chi = 2.0$.

In this study, a steady diffusion flamelet model is included in the combustion model, considering the flame is fully attached to the nozzle. In this approach, the turbulent flame is treated as an ensemble of discrete, small, steady laminar flames, often referred to as diffusion flamelets. Each individual diffusion flamelet is considered to have an identical structure to laminar flames. The hydrogen reaction mechanism of Conaire et al. (2004) was used to create the steady diffusion flamelet. This model includes ten species and 21 steps of reaction. In general, the combustion behavior is insensitive to the reaction mechanism (Fairweather & Woolley 2003).

The conservation equations for laminar flamelets may be formulated as:

$$\rho \frac{\partial Y_i}{\partial t} = \frac{1}{2}\rho\chi \frac{\partial^2 Y_i}{\partial f^2} + S_i \tag{14}$$

$$\rho \frac{\partial T}{\partial t} = \frac{1}{2}\rho\chi \frac{\partial^2 T_i}{\partial f^2} - \frac{1}{C_p}\sum_i H_i S_i + \frac{1}{2C_p}\rho\chi \left[\frac{\partial C_p}{\partial f} + \sum_i C_{p,i}\frac{\partial Y_i}{\partial f}\right]\frac{\partial T}{\partial f} \tag{15}$$

where $C_{p,i}$, H_i, and S_i are the i^{th} element-specific heat, specific enthalpy, and reaction rate, respectively.

2.4. Mesh structure and independence

The computational geometry of the current burner design is chosen as axisymmetric to reduce the computational cost. Three different total numbers of meshes were generated to conduct the independence study, including 16,000, 80,000, and 322,000 cells. The independence test was performed in a flow reacting flow with $C_{1\varepsilon}$=1.6 and $C_{2\varepsilon}$=1.92. The distribution of axial mean temperature among the three mesh structures was very similar, as shown in Fig. 2(a). Hence, based on that, the mesh of 80,000 cells was chosen to perform all simulations in the present work, as depicted in Fig. 2(b). The chosen mesh for the simulations contains minimum orthogonality quality and maximum aspect ratio of 0.9 and 4.4, respectively.

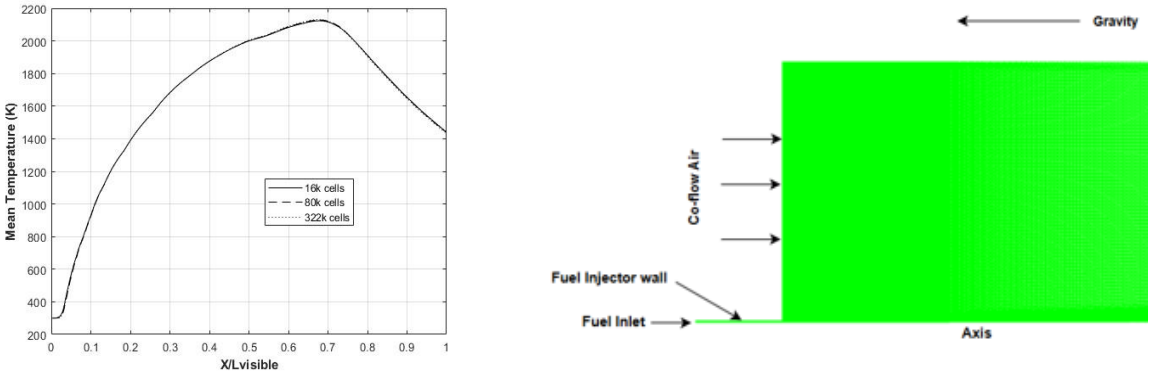

(a) (b)

Fig. 2. (a) Mesh independency test using different total number cells, 16,000, 80,000, and 322,000 cells for the mean temperature at center line axis, (b) Generated 2D axisymmetric structure mesh using 80,000 cells as a base to perform all simulation cases.

3. Results and discussion

3.1. Axial profiles

It can be seen from Fig. 4(a) that the centreline velocity predicted by the modified *k-ε* shows the best results compared to other turbulence models. However, all the turbulence models show under prediction against the experimental data except the modified *k-ε* at $X/L_{flame} > 0.7$. This phenomenon could be induced by the fully developed velocity profile at the injector exit, as mentioned in Tabet-Helal et al. (2006), where the long injector pipe generates a high momentum deficit near the flame core. Despite this, the turbulence model still predicts a reasonable result in the further sections, especially closer to $X/L_{flame} = 1$.

Fig. 4(b) illustrates the prediction of the centerline mean temperature. At $X/L_{flame} = 1/8$, the Modified *k-ε* shows the best agreement to the experiment, while other turbulence models are slightly over-predicted. However, further downstream, the realizable *k-ε* can predict the accurate mean temperature at $X/L_{flame} > 0.3$, while the *k-ε* overpredicts the mean temperature near the maximum flame length. The standard model demonstrates poor accuracy both for centerline momentum and centerline mean temperature while using the Pope Correction, which shows a reasonably good prediction. It is worth mentioning that using the standardized model, the maximum mean temperature is shifted upstream, while using the modified *k-ε* is shifted downstream.

3.2. Radial profiles

The distribution of radial profiles of mean temperature at different measurement locations is shown in Fig. 5. In most locations, all turbulence models predict the maximum mean temperature closer to the air than the experiment, similar to what was reported in Tabet-Helal et al. (2006). However, none of the investigated turbulence models predict the maximum mean temperature where it is located at $X/L_{flame}=1/2$ and $r/R_{fuel}=5$. However, the Pope Correction turbulence models show an adequate prediction compared to others, except near the injector exit, as depicted in Fig. 5(a). In this region, the modified k-ε demonstrates better prediction than other turbulence models. The behavior of hydrogen flame predicted by the Realizable k-ε is most accurate when it is at the centreline of the flame but shows fair consistency over all radial locations.

The prediction of water vapor mass fraction is depicted in Fig. 6. Overall, the Pope Correction turbulence model shows the best agreement with the experimental data except at the $X/L_{flame}=1/8$. Adjustment to the spreading rate using the Pope Correction and differential diffusion might be the key factor here. In Fig. 6(a), the maximum produced H_2O near the injector exit at $r/R_{fuel}=5$ is underpredicted by all the turbulence models. However, further away from the centreline, the modified k-ε shows the best prediction compared to other models. In Fig. 6(b), both modified k-ε and realizable k-ε produce good predictions at $r/R_{fuel}=5$. In Fig. 6(c), all turbulence models show overprediction except for standardized k-ε.

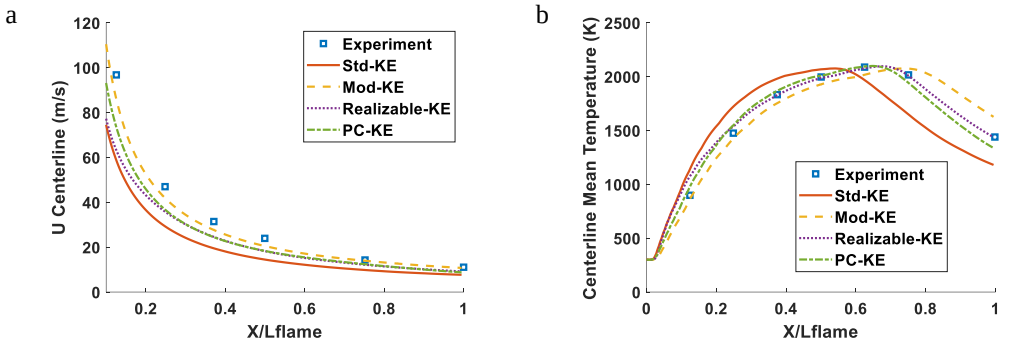

Fig. 4. (a) Centreline velocity, (b) Centreline mean temperature

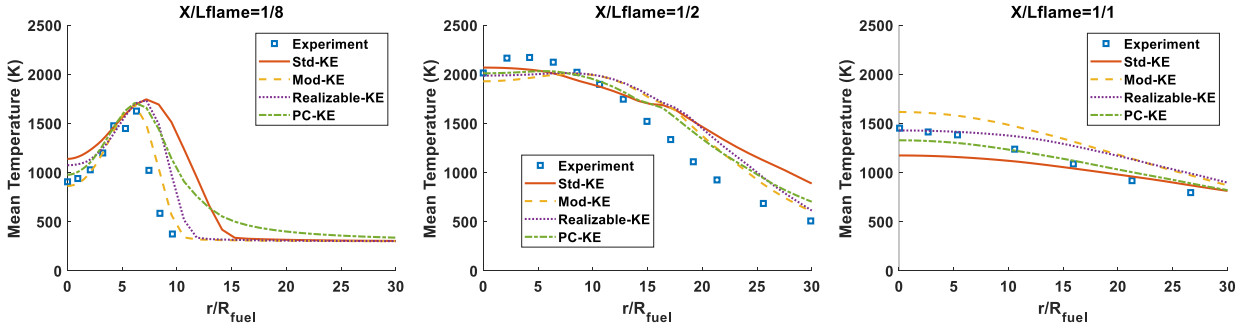

Fig. 5. Mean temperature at different test sections

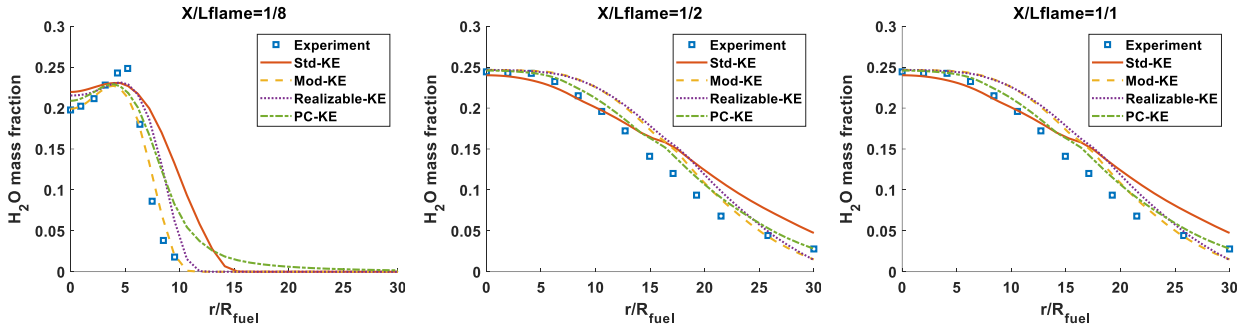

(a) (b) (c)

Fig. 6. H_2O mass fraction at different test sections

4. Conclusions

This study investigates the simulation of non-premixed turbulent hydrogen flames using RANS turbulence models. Four different models are compared, including standardized k-ε, modified k-ε (C_{e1}=1.6), realizable k-ε, and Pope correction model. Steady laminar flamelet and PDF combustion models are adopted to simulate the chemistry and turbulence interaction. Furthermore, the radiation-emitting elements are considered to be water vapor, and DO is the selected radiation model.

Overall, the comparison with experimental data provided from the literature shows good agreement with the numerical results, especially along the axial profiles. It is noted that most turbulence models struggle to achieve highly accurate results due to the inherent over-predictability of RANS models. However, some models can capture good agreement with the experimental data in a specific region. For instance, the realizable k-ε shows the best accuracy at the centerline axis further downstream with a reasonable agreement radially further away. The opposite behavior is noticed in the upstream location. The modified k-ε shows superior ability at the upstream region near the injector exit without the addition of differential diffusion. While the Pope correction improves some of the radial profiles of the RANS model, its overall performance is not better than that of the other simpler models. It is worth mentioning that an additional code to the turbulence model somewhat induces instability in the simulation; hence, a converged result is difficult to attain.

In conclusion, the limited k-ε turbulent model, such as the realizable k-ε model, is found to be a reliable choice for an initial prediction of non-premixed combustion flames, given its reasonable consistency with experimental data and shows notable accuracy for the mean temperature at the centerline region further downstream.

Acknowledgements

The authors thank the Department of Aerospace Engineering, KFUPM, for supporting this research.

References

ANSYS. 2021. Ansys Fluent Theory Guide. (https://www.afs.enea.it/project/neptunius/docs/fluent/html/th/main_pre.htm)

Barlow, R.S. & Carter, C.D. 1994. Raman/Rayleigh/LIF measurements of nitric oxide formation in turbulent hydrogen jet flames. *Combustion and Flame* 97(3–4). 261–280. (doi:10.1016/0010-2180(94)90020-5)

Chen, Lei & Ghoniem, Ahmed F. 2012. Simulation of Oxy-Coal Combustion in a 100 kW $_{th}$ Test Facility Using RANS and LES: A Validation Study. *Energy & Fuels* 26(8). 4783–4798. (doi:10.1021/ef3006993)

Fairweather, M & Woolley, R.M. 2003. First-order conditional moment closure modeling of turbulent, nonpremixed hydrogen flames. *Combustion and Flame* 133(4). 393–405. (doi:10.1016/S0010-2180(03)00025-7)

Fiorina, Benoit. 2019. Accounting for complex chemistry in the simulations of future turbulent combustion systems. *AIAA Scitech 2019 Forum*. San Diego, California: American Institute of Aeronautics and Astronautics. (doi:10.2514/6.2019-0995) (https://arc.aiaa.org/doi/10.2514/6.2019-0995) (Accessed July 1, 2024.)

Habib, Mohamed A. & Abdulrahman, Gubran A.Q. & Alquaity, Awad B.S. & Qasem, Naef A.A. 2024. Hydrogen combustion, production, and applications: A review. *Alexandria Engineering Journal* 100. 182–207. (doi:10.1016/j.aej.2024.05.030)

Larbi, Ahmed Amine & Bounif, Abdelhamid & Senouci, Mohamed & Gökalp, Iskender & Bouzit, Mohamed. 2018. RANS modelling of a lifted hydrogen flame using eulerian/lagrangian approaches with transported PDF method. *Energy* 164. 1242–1256. (doi:10.1016/j.energy.2018.08.073)

Launder, Brian E. & Spalding, Dudley B. 1979. *Lectures in mathematical models of turbulence*. London: Acad. Pr.

Ó Conaire, Marcus & Curran, Henry J. & Simmie, John M. & Pitz, William J. & Westbrook, Charles K. 2004. A comprehensive modeling study of hydrogen oxidation. *International Journal of Chemical Kinetics* 36(11). 603–622. (doi:10.1002/kin.20036)

Oumrani, N. & Aouissi, M. & Bounif, A. & Yssaad, B. & Tabet, F. & Gokalp, I. 2015. A FIRST- AND SECOND-ORDER TURBULENCE MODELS IN HYDROGEN NON-PREMIXED FLAM. *International Journal of Heat and Technology* 33(3). 27–34. (doi:10.18280/ijht.330304)

Peters, Norbert. 2001. Turbulent Combustion. *Measurement Science and Technology* 12(11). 2022–2022. (doi:10.1088/0957-0233/12/11/708)

Pitsch, H. & Peters, N. 1998. A Consistent Flamelet Formulation for Non-Premixed Combustion Considering Differential Diffusion Effects. *Combustion and Flame* 114(1–2). 26–40. (doi:10.1016/S0010-2180(97)00278-2)

Pope, S. B. 1978. An explanation of the turbulent round-jet/plane-jet anomaly. *AIAA Journal* 16(3). 279–281. (doi:10.2514/3.7521)

Shih, Tsan-Hsing & Liou, William W. & Shabbir, Aamir & Yang, Zhigang & Zhu, Jiang. 1995. A new k-ϵ eddy viscosity model for high reynolds number turbulent flows. *Computers & Fluids* 24(3). 227–238. (doi:10.1016/0045-7930(94)00032-T)

Tabet, F. & Sarh, B. & Gökalp, I. 2011. Turbulent non-premixed hydrogen-air flame structure in the pressure range of 1–10 atm. *International Journal of Hydrogen Energy* 36(24). 15838–15850. (doi:10.1016/j.ijhydene.2011.08.064)

Tabet-Helal, F. & Sarh, B. & Menou, A. & Gökalp, I. 2006. A COMPARATIVE STUDY OF TURBULENCE MODELLING IN HYDROGEN-AIR NONPREMIXED TURBULENT FLAMES. *Combustion Science and Technology* 178(10–11). 1887–1909. (doi:10.1080/00102200600790896)